Modeling and Analysis of Rotary Mechanical Systems Linked Through a U-joint

Masoud SoltanRezaee and Mohammad-Reza Ghazavi
Department of Mechanical Engineering, Tarbiat Modares University, Tehran, Iran
Email: m.soltan@modares.ac.ir, ghazavim@modares.ac.ir

Asghar Najafi
Department of Mechanical Rotary Equipment, Niroo Research Institute, Tehran, Iran
Email: anajafi@nri.ac.ir

Wei-Hsin Liao
Department of Mechanical and Automation Engineering, The Chinese University of Hong Kong, Hong Kong, China
Email: whliao@cuhk.edu.hk

***Abstract*—Utilizing the U-joint is the most usual and familiar way to connect rotating shafts, which are at an angle with each other. Although, this mechanical coupling has various advantages, converts a constant input velocity to a fluctuating output one. Consequently, this produces resonance conditions in the power transmission system of vehicles. In this study, the vibrations of drivetrains are considered to examine the system torsional behaviors. Here, the derived mathematical model is investigated by means of Floquet theory. Furthermore, the acquired results are validated analytically by applying the frequency analysis. In order to examine the influence of different parameters on the vibrations, the unstable zones are identified and analyzed. In addition, the effects of joint angle and shaft length are investigated. The obtained model is useful to simulate the torsional behaviors of various two-axis power transmission systems and identify the resonance conditions.**

***Index Terms*—rotary systems, analysis, system modeling, vibration**

I. Introduction

A well-known purpose of rotating shaft systems is in the transfer of torque and power between two objects in different rotary systems [1-7]. There are several mechanisms, which allow move transfer under some limitations depending on the distance and angle between the driver and driven shafts. Applying the universal joint is a classical solution that used in many mechanisms and systems in several industries [8]. Nowadays, this non-constant velocity joint is applied as a key component of several powertrain systems, for example, in on-road and off-road vehicles, rail cars, robotics, shipping industries, and other power transmission systems [9, 10].

Universal joints are a type of couplings that permit the shaft fixed on them to bend in almost any directions. This mechanical coupling is composed of a pair of hinges located close and perpendicular to each other, linked by a cross shaft. Generally, in rotary machines, U-joints are used between intersecting axes and are common due to their excellent features such as high torque and operating angle capacity, effective cost, high reliability and simplicity [10]. Although the first shaft has a constant input speed, there will be a fluctuating output speed. As a result, the driveline is stimulated and there are many unstable areas in the system [4, 11]. Recently, some researchers have been considered the torsional oscillations transmitted from the flywheel to the drivetrain, which induce a plethora of noise, vibration and harshness concerns in Front Wheel Drive (FWD) vehicles [12-16]. Moreover, torsional vibrations in Rear Wheel Drive (RWD) cars, where the nonlinear behavior of the non-constant velocity U-joint plays a significant role, must be analyzed. Using finite element analysis (FEA) can be beneficial to model and investigate the drivelines. Recently lateral vibrations of a driveline interconnected by two U-joints have been examined to determine the bending motions and harmonic resonances of the systems [17]. Furthermore, transverse oscillations of a multi-body system have been studied to obtain the natural frequencies and mode shapes of the system, where the lumped mass shafts have been linked with multiple hinges [18]. Jayanaidu et al. [19] have numerically optimized the design and structure of a drive shaft connected with two couplings by using software ANSYS. In addition, optimization of system parameters was the main concept of some multi-joint machines that simulated via different FE models [20, 21].

All the mentioned works prepare a solid motivation to investigate torsional vibrations of driveline systems via the finite element method. In almost all of these studies, the characteristics of rotating shafts have been estimated by massless or lumped mass systems. In general, by using a FE model, prediction of unstable regions of drivelines is possible. To the best knowledge of the authors,

Manuscript received April 24, 2018; revised March 15, 2019.

© 2019 Int. J. Mech. Eng. Rob. Res

doi: 10.18178/ijmerr.8.3.459-465

simulation of the powertrains by considering the shaft inertia via analytical schemes has not been carried out yet. Therefore, we provide a mathematical model for shaft systems, which is useful to consider numerous rotary systems. In driveline shafts, the whole mechanism is physically stimulated via an angular periodically fluctuating excitation that can be accounted as internal stimulation. In this model, the working angle of universal coupling has no limitations except geometric constraint at 90^{o}. It means that mathematical relations are valid for any angled shafts and the presented FE model is general. Note that some mentioned relations for the transfer speed of U-joints, which are almost linear, are acceptable just for small angles. In this research, the equations of motion consist of a set of Mathieu type equations. Moreover, the system stability has been analyzed via numerical Floquet theory. Finally, the results prove the importance of considering the continuous model and successful application of the finite element method in the analysis of drivelines.

II. Model

A. Development of Model

The presented power transmission system, which consists of elastic rotating shafts, is simulated by means of a distributed parameter model. The system is driven by an input speed that transfers from an electric motor (Fig. 1). However, each shaft is aligned; they are in angle (α) with each other, so have been linked via a mechanical coupling. Let each shaft has mass density ρ_i, polar area moment of inertia I_i, shear modulus G_i, Rayleigh damping coefficients of inertia and stiffness a_i and b_i, respectively, vectors of nodal torsional coordinates of the first and second shaft are $\boldsymbol{\theta}$ and $\boldsymbol{\varphi}$, respectively, mass matrix $\mathbf{M}$, stiffness matrix $\mathbf{K}$, angular velocity Ω_i, torque $T_{in\,i}$ and length l_i. It should be noted that a universal coupling has three main parts, two yokes, and a crosspiece. The following assumptions are made to reduce the behavior of the driveline system to the presented model:

i. Each shaft is uniform and symmetric across its axis.
ii. The shaft system is only loaded in the torsion.
iii. The U-joint does not have any clearance and friction.
iv. The yoke mass can be modeled via a solid disk (J_d).
v. The crosspiece mass is negligible regarding the parts-mass.
vi. The input angular speed (Ω_0) of the system is constant.

B. Equations of Motion

The torsional equations of motion can be derived analytically from a combination technique. Herein, equations of motion for dynamics of each shaft can be written as

$$\begin{aligned}&\left(\rho_1 I_1 l_1 \mathbf{M_1} + J_d \mathbf{u_{2p}} \mathbf{u_{2p}^T}\right)\ddot{\boldsymbol{\theta}} \\ &+\left(a_1\left(\rho_1 I_1 l_1\right)\mathbf{M_1} + b_1\left(\frac{G_1 I_1}{l_1}\right)\mathbf{K_1}\right)\dot{\boldsymbol{\theta}} \\ &+\frac{G_1 I_1}{l_1}\mathbf{K_1}\boldsymbol{\theta} = T_{in1}\mathbf{u_{2p}},\end{aligned} \tag{1}$$

$$\begin{aligned}&\left(\rho_2 I_2 l_2 \mathbf{M}_2 + J_d \mathbf{v_1}\left(\mathbf{v_1^T} + \mathbf{v_{2q+1}^T}\right)\right)\ddot{\boldsymbol{\varphi}} \\ &+\left(a_2\left(\rho_2 I_2 l_2\right)\mathbf{M}_2 + b_2\left(\frac{G_2 I_2}{l_2}\right)\mathbf{K}_2\right)\dot{\boldsymbol{\varphi}} \\ &+\frac{G_2 I_2}{l_2}\mathbf{K}_2\boldsymbol{\varphi} = T_{in2}\mathbf{v_{2q+1}}.\end{aligned} \tag{2}$$

Note that the shafts are taken as separate parts with p and q equal-length elements. The unit vectors ($\mathbf{u}_i$ and $\mathbf{v}_i$) in addition to the mass and stiffness matrices are introduced as (p and q =1)

$$\mathbf{u_1} = \begin{Bmatrix}1\\0\end{Bmatrix}, \mathbf{u}_2 = \begin{Bmatrix}0\\1\end{Bmatrix}, \tag{3}$$

$$\mathbf{v_1} = \begin{Bmatrix}1\\0\\0\end{Bmatrix}, \mathbf{v_2} = \begin{Bmatrix}0\\1\\0\end{Bmatrix}, \mathbf{v_3} = \begin{Bmatrix}0\\0\\1\end{Bmatrix}, \tag{4}$$

$$\boldsymbol{\theta} = \begin{Bmatrix}\theta_1\\\theta_2\end{Bmatrix}, \boldsymbol{\varphi} = \begin{Bmatrix}\varphi_0\\\varphi_1\\\varphi_2\end{Bmatrix}. \tag{5}$$

$$\begin{aligned}\mathbf{M}_{fixed-free} &= \mathbf{M}_1 = \frac{1}{30}\begin{bmatrix}16 & 2\\2 & 4\end{bmatrix},\\ \mathbf{M}_{free-free} &= \mathbf{M}_2 = \frac{1}{30}\begin{bmatrix}5 & 2 & -1\\20 & 16 & 2\\5 & 2 & 4\end{bmatrix},\end{aligned} \tag{6}$$

$$\begin{aligned}\mathbf{K}_{fixed-free} &= \mathbf{K}_1 = \frac{1}{3}\begin{bmatrix}16 & -8\\-8 & 7\end{bmatrix},\\ \mathbf{K}_{free-free} &= \mathbf{K}_2 = \frac{1}{3}\begin{bmatrix}0 & -8 & 1\\0 & 16 & -8\\0 & -8 & 7\end{bmatrix},\end{aligned} \tag{7}$$

It is worth mentioning that based on the sixth assumption, θ_0=0. Moreover, the left and right ends of the driving shaft are fixed and free, respectively. However, the driven shaft is a free-free rotating shaft in such a configuration.

© 2019 Int. J. Mech. Eng. Rob. Res

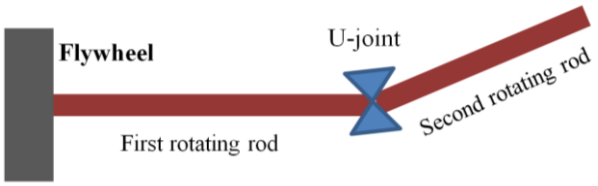

Figure 1. Schematic of prepared model for the power transmission systems

The relation of velocity ratio of U-joint (η_1) is nonlinear and stated as [10]

$$\eta_1 = \frac{T_{in1}}{T_{out1}} = \frac{\Omega_{out1}}{\Omega_{in1}} = \frac{\dot{\varphi}_{0,t}}{\dot{\theta}_{2p,t}} = \frac{\cos\alpha}{1-\sin^2\alpha\sin^2\left(\Omega_0 t+\theta_{2p}\right)}. \tag{8}$$

So

$$\dot{\varphi}_0 = \eta_1\Omega_0 + \eta_1\dot{\theta}_{2p} \rightarrow \ddot{\varphi}_0 = \dot{\eta}_1\Omega_0 + \dot{\eta}_1\dot{\theta}_{2p} + \eta_1\ddot{\theta}_{2p}. \tag{9}$$

The equations can be linearized as

$$\eta_1 \approx \eta_1\big|_{\theta_{2p}=0} + \left.\frac{\partial\eta_1}{\partial\theta_{2p}}\right|_{\theta_{2p}=0}\theta_{2p} = \eta_{01} + \dot{\eta}_{01}\frac{1}{\Omega_0}\theta_{2p}, \tag{10}$$

where

$$\eta_{01} = \frac{\cos\alpha}{1-\sin^2\alpha\sin^2\theta_0}, \tag{11}$$

also

$$\left.\frac{\partial^2\eta_1}{\partial\theta_{2p,t}^{\ 2}}\right|_{\theta_{2p}=0} = \frac{1}{\Omega_0^2}\ddot{\eta}_{01}, \tag{12}$$

so

$$\dot{\eta}_1 \approx \frac{\partial\eta_1}{\partial\theta_{2p,t}}\dot{\theta}_{2p,t} \approx \left(\left.\frac{\partial\eta_1}{\partial\theta_{2p,t}}\right|_{\theta_{2p}=0} + \left.\frac{\partial^2\eta_1}{\partial\theta_{2p,t}^2}\right|_{\theta_{2p}=0}\theta_{2p}\right)(\Omega_0+\dot{\theta}_{2p}) \approx \dot{\eta}_{01} + \frac{\ddot{\eta}_{01}}{\Omega_0}\theta_{2p} + \frac{\dot{\eta}_{01}}{\Omega_0}\dot{\theta}_{2p}. \tag{13}$$

C. Equations with Dimensionless Parameters

It is more convenient to write the governing equations in dimensionless form. To this end, the torsional coordinate's derivatives with respect to non-dimensional time are recomputed accordingly

$$\dot{\mathrm{O}} = \frac{d}{dt}\mathrm{O} = \frac{d}{d\tau}\mathrm{O}\frac{d\tau}{dt} = \mathrm{O}'\Omega_0 \rightarrow \ddot{\mathrm{O}} = \mathrm{O}''\Omega_0^2. \tag{14}$$

and the following dimensionless parameters are introduced as

$$\zeta = \frac{c_{k1}}{2\sqrt{k_1 J_1}}, \Omega = \Omega_0\sqrt{\frac{J_1}{k_1}}, \vartheta_2 = \frac{b_2}{b_1}, \gamma_2 = \frac{J_2}{J_1}, \lambda = \frac{J_d}{J_1}, \mu_2 = \frac{k_2}{k_1}, \tau = \Omega_0 t, \nu_1 = \frac{c_{m1}}{c_{k1}}, \nu_2 = \frac{c_{m2}}{c_{k2}}, T_{0in1} = \frac{T_{in1}}{k_1}, T_{0out1} = \frac{T_{out1}}{k_1}, \tag{15}$$

where

$$J_1 = \rho_1 I_1 l_1, J_2 = \rho_2 I_2 l_2, c_{m1} = a_1 J_1, c_{m2} = a_2 J_2, c_{k1} = b_1 k_1, c_{k2} = b_2 k_2, k_1 = \frac{G_1 I_1}{l_1}, k_2 = \frac{G_2 I_2}{l_2}. \tag{16}$$

In the following, the torsional coordinate's derivations of some parameters are calculated

$$\varphi_0' = \eta_1\left(1+\theta_{2p}'\right) = \eta_{01} + \eta_{01}'\theta_{2p} + \eta_{01}\theta_{2p}', \varphi_0'' = \eta_1'\left(1+\theta_{2p}'\right) + \eta_1\theta_{2p}'' = \eta_{01}' + \eta_{01}''\theta_{2p} + 2\eta_{01}'\theta_{2p}' + \eta_{01}\theta_{2p}''. \tag{17}$$

The equations of motion for torsional vibrations of the presented powertrain system model can now be expressed as

$$\left(\mathbf{M_1} + \lambda\mathbf{u_{2p}}\mathbf{u_{2p}^T}\right)\boldsymbol{\theta}'' + \frac{1}{\Omega^2}\mathbf{K_1}\boldsymbol{\theta} + \frac{2\zeta}{\Omega}\left(\nu_1\mathbf{M_1} + \mathbf{K_1}\right)\boldsymbol{\theta}' = \frac{1}{\Omega^2}T_{0in1}\mathbf{u_{2p}}, \tag{18}$$

$$\left(\mathbf{M}_2 + \lambda\gamma_2\mathbf{v_1}\left(\mathbf{v_1^T} + \mathbf{v_{2q+1}^T}\right)\right)\boldsymbol{\varphi}'' + \frac{1}{\Omega^2}\frac{\mu_2}{\gamma_2}\mathbf{K}_2\boldsymbol{\varphi} + \frac{2\zeta}{\Omega}\frac{\vartheta_2\mu_2}{\gamma_2}\left(\nu_2\mathbf{M}_2 + \mathbf{K}_2\right)\boldsymbol{\varphi}' = -\frac{1}{\Omega^2}\frac{T_{0out1}\mathbf{v_1}}{\gamma_2}. \tag{19}$$

Finally, the matrix–vector form of the whole system can be written as

$$\frac{\mathbf{M}}{5}\begin{Bmatrix}\theta_1''\\ \theta_2''\\ \varphi_1''\\ \varphi_2''\end{Bmatrix} + \frac{2\zeta}{5\Omega}\mathbf{C}\begin{Bmatrix}\theta_1'\\ \theta_2'\\ \varphi_1'\\ \varphi_2'\end{Bmatrix} + \frac{2\mathbf{K}}{\Omega^2}\begin{Bmatrix}\theta_1\\ \theta_2\\ \varphi_1\\ \varphi_2\end{Bmatrix} = \mathbf{N}, \tag{20}$$

$$\mathrm{M}_{11} = \mathrm{M}_{33} = 16, \mathrm{M}_{12} = \mathrm{M}_{21} = \mathrm{M}_{34} = \mathrm{M}_{43} = 2, \mathrm{M}_{32} = 20\eta_{01}, \mathrm{M}_{22} = 4 + 5\gamma_2\eta_{01}^2 + 30\lambda\left(1+\gamma_2^2\eta_{01}^2\right), \mathrm{M}_{23} = 2\gamma_2\eta_{01}, \mathrm{M}_{44} = 4, \mathrm{M}_{24} = \gamma_2\eta_{01}\left(30\lambda\gamma_2 - 1\right), \mathrm{M}_{42} = 5\eta_{01}; \text{other } \mathrm{M}_{ij} = 0. \tag{21}$$

© 2019 Int. J. Mech. Eng. Rob. Res

$$
\begin{aligned}
&C_{11}=16\nu_1+160, C_{32}=20\left(\eta'_{01}\,\Omega/\zeta+\eta_{01}\vartheta_2\mu_2\,\nu_2/\gamma_2\right),\\
&C_{12}=C_{21}=2\nu_1-80, C_{24}=\left(10-\nu_2\right)\vartheta_2\mu_2\eta_{01},\\
&C_{22}=5\left(\gamma_2\eta_{01}\eta'_{01}\,\Omega/\zeta+\vartheta_2\mu_2\nu_2\eta_{01}^2\right)+30\lambda\gamma_2^2\eta_{01}\eta'_{01}\,\Omega/\zeta\\
&+4\nu_1+70, C_{34}=C_{43}=\left(2\nu_2-80\right)\vartheta_2\,\mu_2/\gamma_2,\\
&C_{23}=\left(2\nu_2-80\right)\vartheta_2\mu_2\eta_{01}, C_{33}=16\left(\nu_2+10\right)\vartheta_2\,\mu_2/\gamma_2,\\
&C_{42}=5\left(\vartheta_2\mu_2\nu_2\eta_{01}+\gamma_2\eta'_{01}\,\Omega/\zeta\right)/\gamma_2,\\
&C_{44}=\left(4\vartheta_2\mu_2\nu_2+70\vartheta_2\mu_2\right)/\gamma_2;\text{other}\quad C_{ij}=0.
\end{aligned}
\tag{22}
$$

$$
\begin{aligned}
&K_{11}=16, K_{12}=K_{21}=-8, K_{23}=-8\mu_2\eta_{01}, K_{24}=\mu_2\eta_{01},\\
&K_{22}=7+\left(\eta_{01}\eta''_{01}+\eta'^2_{01}\right)\gamma_2/2+3\lambda\gamma_2^2\left(\eta_{01}\eta''_{01}+\eta'^2_{01}\right)\Omega^2\\
&+\zeta\Omega\vartheta_2\mu_2\nu_2\eta_{01}\eta'_{01}, K_{34}=K_{43}=-8\,\mu_2/\gamma_2,\\
&K_{32}=4\zeta\Omega\vartheta_2\nu_2\eta'_{01}\,\mu_2/\gamma_2+2\eta''_{01}\Omega^2,\\
&K_{42}=\left(2\zeta\vartheta_2\nu_2\mu_2\eta'_{01}+\eta''_{01}\gamma_2\Omega\right)\Omega/2\gamma_2,\\
&K_{33}=16\,\mu_2/\gamma_2, K_{44}=7\,\mu_2/\gamma_2;\text{other}\quad K_{ij}=0.
\end{aligned}
\tag{23}
$$

$$
\begin{aligned}
&N_{1\times1}=0,\\
&N_{2\times1}=-2\vartheta_2\mu_2\nu_2\eta_{01}^2\,\zeta/\Omega-\gamma_2\eta_{01}\eta'_{01}\left(1+6\gamma_2\lambda\right),\\
&N_{3\times1}=-4\eta'_{01}-8\vartheta_2\mu_2\nu_2\eta_{01}\,\zeta/\left(\Omega\gamma_2\right),\\
&N_{4\times1}=-\eta'_{01}-2\eta_{01}\vartheta_2\mu_2\nu_2\,\zeta/\left(\Omega\gamma_2\right).
\end{aligned}
\tag{24}
$$

III. Analysis

Equation (20) is for the governing equations of torsional motion of the model. A display of the Eq. (20), which is more convenient for stability analysis, can be given as

$$
\begin{Bmatrix}\theta'_1\\ \theta'_2\\ \varphi'_1\\ \varphi'_2\\ \theta''_1\\ \theta''_2\\ \varphi''_1\\ \varphi''_2\end{Bmatrix}=\begin{bmatrix}\mathbf{0} & \mathbf{I}\\ \dfrac{10\mathbf{K}}{-\mathbf{M}} & \dfrac{2\zeta\mathbf{C}}{-\mathbf{M}}\end{bmatrix}\begin{Bmatrix}\theta_1\\ \theta_2\\ \varphi_1\\ \varphi_2\\ \theta'_1\\ \theta'_2\\ \varphi'_1\\ \varphi'_2\end{Bmatrix},
\tag{25}
$$

In this work, the dynamic stability of the system is investigated point-by-point by means of a numerical method [22]. It is able to determine the stability areas and resonance conditions of a shaft system with parametric excitation.

It is clear that the location of instability regions (resonance areas) on different stability figures depends on the natural frequencies of the shaft system. In such excited systems, the parametric resonance zones can be given by

Combinational difference– type :

$$
\begin{aligned}
&\Omega_{CD,ijk}=\frac{\omega_j-\omega_i}{2k},\\
&\text{Combinational sum}-\text{type}:\Omega_{CS,ijk}=\frac{\omega_j+\omega_i}{2k},\\
&\text{Harmonic}:\Omega_{H,ik}=\frac{\omega_i}{2k},\\
&\text{Subharmonic}:\Omega_{S,ik}=\frac{\omega_i}{2k-1},\\
&j>i; i,j=1,2,3,4; k=1,2.
\end{aligned}
\tag{26}
$$

IV. Results And Discussions

In order to verify the results, the obtained outputs will be compared. The analytical results are obtained by substituting the frequencies in Eq. (26) and the numerical results are obtained by Floquet theory.

A. Analytical Results

In Table 1, the values of the four first natural frequencies are mentioned to carry out the frequency analysis. The parametric resonance zones related to the fundamental frequencies of driveline are reported in Table 2 in detail.

The analysis of dynamic stability is carried out via the numerical Floquet theory. Fig. 2 illustrates the results of stability analysis where the shaded points show the unstable points. The vertical axis displays the coupling angle α in rad, and the horizontal axis depicts the non-dimensional angular velocity Ω.

TABLE I. TORSIONAL NATURAL FREQUENCIES OF THE SHAFT SYSTEM BASED ON THE MODEL

Natural frequencies	Value
First	0.786
Second	2.395
Third	4.389
Fourth	7.048

TABLE II. CALCULATED LOCATIONS OF FIRST ORDER RESONANCES BASED ON FREQUENCY ANALYSIS

Res.	Harmonic	Sub-harm.	Comb. Res.	Sum-type	Diff.-type
Ω_{11}	0.393	0.786	Ω_{121}	1.591	0.805
Ω_{21}	1.198	2.395	Ω_{131}	2.588	1.802
Ω_{31}	2.195	4.389	Ω_{141}	3.917	3.131
Ω_{41}	3.524	7.048	Ω_{231}	3.392	0.997
			Ω_{241}	4.722	2.327
			Ω_{341}	5.719	0.665

Certain instability regions, which are previously calculated analytically, are labeled in Fig. 2. Fig. 2 demonstrates that the results as reported in Table II, are in

© 2019 Int. J. Mech. Eng. Rob. Res

an excellent agreement with the numerical ones. As a result, a more accurate investigation, which shows the effect of other modes, can be performed.

One of the most remarkable factors that has been evaluated here is the system geometry. The system geometry includes the joint angle and the shaft length. These factors normally affect the stability significantly and should be checked. The results are charts, which include a pair of the present model parameters and show the system stability.

B. Joint Angle

In order to evaluate the effect of the joint angle at different geometries, two different lengths are considered for the shafts. Therefore, the length of the second shaft is not equal to the first one (Fig. 3). Generally, by increasing the angle from zero (where no excitation exists), the unstable zones extend and become wider. It is observed that different types of instability regions are revealed. The resonances, which are associated with lower vibrational mode, have more clarity. Usually, the peaks corresponding to higher system natural frequencies occur in high misalignment (e.g. $\Omega_{H,22}$ and $\Omega_{S,22}$). Furthermore, by increasing the angle of misalignment (the angle between intersecting shaft axes), new unstable areas emerge that are not practically important. On the other hand, there are unstable areas close together at high angles; hence, they are not clearly identifiable.

By comparison, between Figs. 3a, 3b and 2, it can be observed that as the driven shaft length increases, the peaks shift toward a lower velocity that should be considered in the design. It is because the resonance conditions are related to the system frequencies. As a result, increasing the second shaft length leads to an increase in the equivalent length of the whole system. By analyzing graphs, it can be deduced that increasing the driven shaft length can have a stabilizing effect. In other words, by decreasing l_2, unstable regions will be in a wider range of velocity and even at higher velocities, there are several resonance conditions.

C. Shaft Length

Fig. 4 exhibits another stability diagram in which the coupling joint angle α is fixed. In this diagram, the vertical axis shows the ratio of the second to the first shaft length at different angles. Here, the qualitative analysis is more important than quantitative analysis.

By analysing graph, it can be found that the system geometry, including joint angle and shaft length, has apparent influences on resonance zones. Moreover, this parameter variation leads to changes in the natural frequencies (because the zones are not parallel to the vertical axis), that shift the peaks of resonance zones toward the left. It is the result of increasing the convergence of natural frequencies.

Another significant issue in Fig. 4 is that the displacement of unstable areas is gradually decreased by increasing the length ratio. In other words, the parallelism of the instability zones with the vertical axis is further in the top of the diagram. Moreover, as the driving shaft length increased, the unstable areas will be developed especially at higher velocity range. By comparison of Figs. 4a and 4b, it can be seen that by increasing the joint angle, the shaded zones will become wider and even some unstable areas will emerge, which should be considered in the analysis. The other results are the same as mentioned in the discussions of Fig. 3.

V. Conclusion

In this study, an excited drivetrain was modeled mathematically and the resonance conditions were investigated. The studied machine includes two rotating shafts connected by an ideal massless U-joint. Here, the system torsional equations of motion consist of a set of differential equations. Furthermore, the numerical results have been shown in the stability diagrams graphically. Finally, the instability conditions were analyzed quantitative and qualitative. The results are as follows:

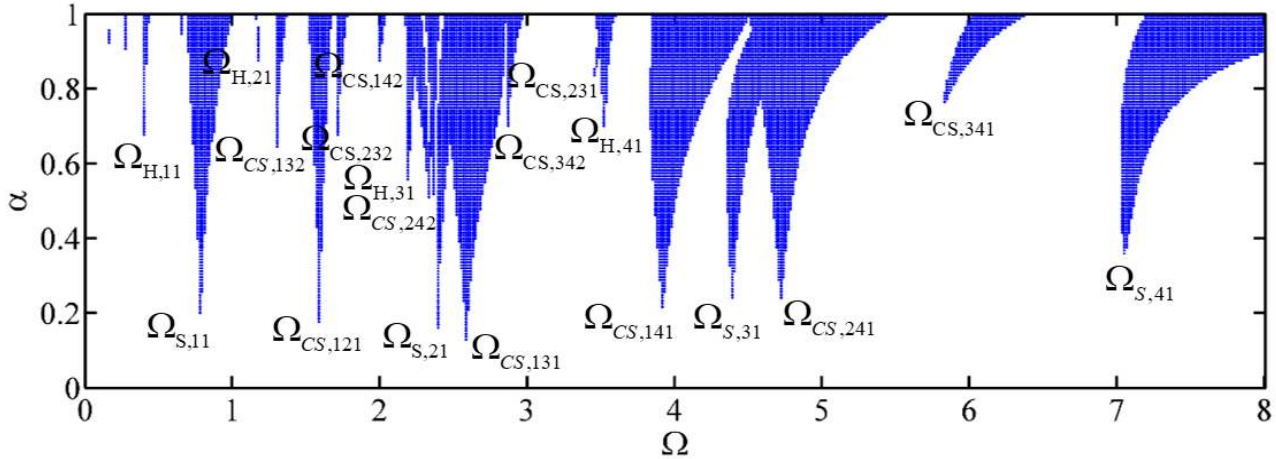

Figure 2. Comparison of numerical and analytical results (the term α represents the joint angle in radian)

© 2019 Int. J. Mech. Eng. Rob. Res

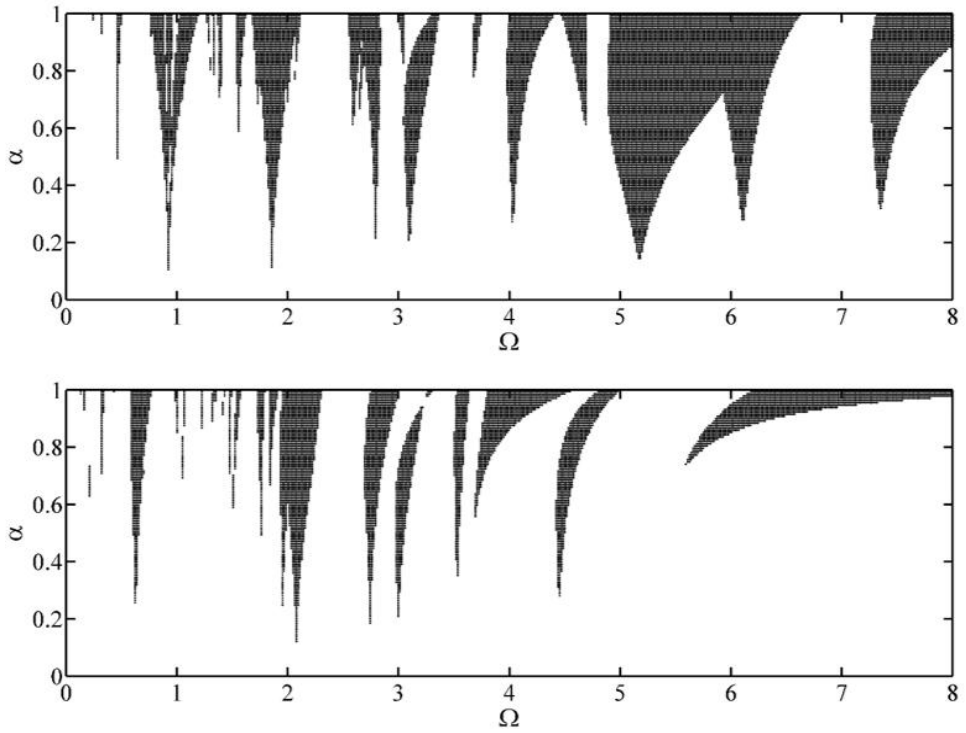

Figure 3. Effect of joint angle (α) and shaft length on the stability, a: $l_2 = 0.7\ l_1$, b: $l_2 = 1.5\ l_1$

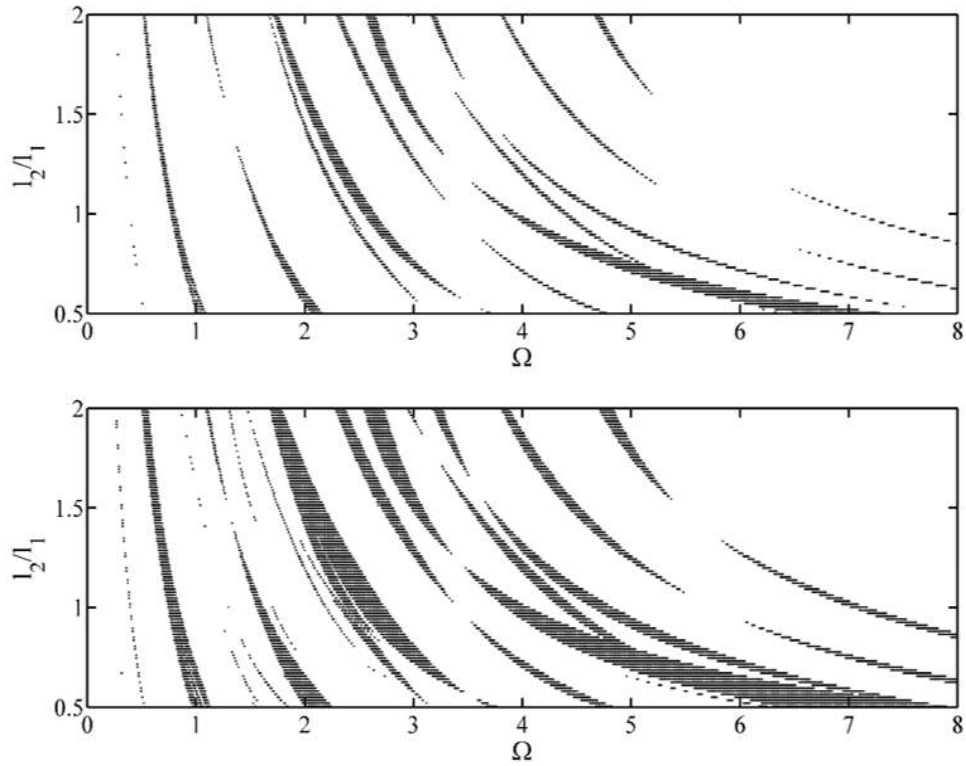

Figure 4. Effect of shaft length on the stability, a: $\alpha = 0.4$ rad, b: $\alpha = 0.8$ rad

- Increasing the input velocity and joint angle causes less stability in general. Moreover, by increasing the joint angle, new unstable zones appear especially at some large angles.
- Increasing the length ratio (driven shaft length) and joint angle makes the instability areas wider.
- By changing the system geometry, stabilizing the system is possible, which should be considered in the design, modeling, and operation of such systems.
- The model is useful to consider the behaviors of various power transmission systems and identify different types of resonance conditions.

© 2019 Int. J. Mech. Eng. Rob. Res

REFERENCES

[1] M. S. Rezaee, A. A. Jafari, and M. R. Ghazavi, "Dynamic stability of a system including three shafts," in *Proc. Second Int. Conf. on Adv. in Robotic, Mechanical Eng. and Design (ARMED 2012)*, Dubai, UAE, September 20-21.

[2] M. SoltanRezaee, M. R. Ghazavi, and A. Najafi, "Parametric resonances for torsional vibration of excited rotating machineries with nonconstant velocity joints," *Journal of Vibration and Control*, vol. 24, no. 15, pp. 3262–3277, 2017.

[3] M. SoltanRezaee, M. Afrashi, and S. Rahmanian, "Vibration analysis of thermoelastic nano-wires under coulomb and dispersion forces," *International Journal of Mechanical Sciences*, 142-143, pp. 33-43, 2018.

[4] M. SoltanRezaee and M. R.Ghazavi, "Thermal, size and surface effects on the nonlinear pull-in of small-scale piezoelectric actuators," *Smart Materials and Structures*, vol. 26, no. 9, p. 065023, 2017.

[5] M. SoltanRezaee and M. R. Ghazavi, "Obtaining stable cardan angles in rotating systems and investigating the effective parameters on system stability," *Modares Mechanical Engineering*, vol. 14, no. 12, pp. 163-170. (in Persian), 2015.

[6] M. SoltanRezaee, M. R. Ghazavi, and A. Najafi, "Mathematical modelling for vibration evaluation of powertrain systems," *Modelling, Simulation and identification (MSI 2017)*, P. Chen, and M. Hamza, eds., Acta Press, Calgary, Canada, pp. 73–79, 2017.

[7] M. SoltanRezaee, M. R. Ghazavi, A. Najafi, and S. Rahmanian, , 2018, "Stability of a multi-body driveshaft system excited through U-joints," *Meccanica*, vol. 53, no. 4, pp. 1167-1183.

[8] F. Vesali, M. A. Rezvani, and M. Kashfi, "Dynamics of universal joints, its failures and some propositions for practically improving its performance and life expectancy," *Journal of Mechanical Science and Technology*, vol. 26, no. 8, pp. 2439-2449, 2012.

[9] M. Zajíček and J. Dupal, "Analytic solution of simplified Cardan's shaft model," *Applied and Computational Mechanics*, vol. 8, pp. 215–228, 2014.

[10] H. C. Seherr-Thoss, F. Schmelz, and E. Aucktor, Universal joints and driveshafts: Analysis, design, applications, Springer Science & Business Media, 2006.

[11] A. Mazzei, A. Argento, and R. Scott, "Dynamic stability of a rotating shaft driven through a universal joint," *Journal of Sound and Vibration*, vol. 222, no. 1, pp. 19-47, 1999.

[12] A. Haris, E. Motato, M. Mohammadpour, S. Theodossiades, H. Rahnejat, O' Mahony, M., A. F. Vakakis, L. A. Bergman, and D. M. McFarland, "On the effect of multiple parallel nonlinear absorbers in palliation of torsional response of automotive drivetrain," *International Journal of Non-Linear Mechanics, 96(Supplement C)*, pp. 22-35, 2017.

[13] A. Haris, E. Motato, S. Theodossiades, H. Rahnejat, P. Kelly, A. Vakakis, L. A. Bergman, and D. M. McFarland, "A study on torsional vibration attenuation in automotive drivetrains using absorbers with smooth and non-smooth nonlinearities," *Applied Mathematical Modelling*, 46(Supplement C), pp. 674-690, 2017.

[14] E. Motato, A. Haris, S. Theodossiades, M. Mohammadpour, H. Rahnejat, P. Kelly, A. Vakakis, D. McFarland, and L. Bergman, "Targeted energy transfer and modal energy redistribution in automotive drivetrains," *Nonlinear Dynamics*, vol. 87, no. 1, pp. 169-190, 2017.

[15] P. Bingham, S. Theodossiades, T. Saunders, E. Grant, and R. Daubney, 2016, "A study on automotive drivetrain transient response to 'clutch abuse' events," in *Proc. the Institution of Mechanical Engineers, Part D: Journal of Automobile Engineering*, vol. 230, no. 10, pp. 1403-1416.

[16] A. T. El-Sayed, and H. S. Bauomy, "Passive and active controllers for suppressing the torsional vibration of multiple-degree-of-freedom system," *Journal of Vibration and Control*, vol. 21, no. 13, pp. 2616-2632, 2015.

[17] M. Browne and A. Palazzolo, "Super harmonic nonlinear lateral vibrations of a segmented driveline incorporating a tuned damper excited by non-constant velocity joints," *Journal of Sound and Vibration*, vol. 323, no. 1, pp. 334-351, 2009.

[18] J. Iqbal and M. S. Qatu, "Transverse vibration of multi-segment shaft system joined with multiple hinges," *International Journal of Vehicle Noise and Vibration*, vol. 6, no. 1, pp. 73-89, 2010.

[19] P. Jayanaidu, M. Hibbatullah, and P. Baskar, "Analysis of a drive shaft for automobile applications," *IOSR Journal of Mechanical and Civil Engineering (IOSR-JMCE)*, vol. 10, pp. 43-46, 2013.

[20] H. S. Song, W. K. Shi, Y. Long, F. X. Guo, and D. G. Fang, "Multi-universal coupling phase modeling and optimization base on floor vibration control," *Proc. Key Engineering Materials, Trans Tech Publ*, pp. 669-675.

[21] H. Y. Yuan, "Based on analysis of finite element analysis of automobile transmission shaft comprehensive optimization," *Proc. Applied Mechanics and Materials, Trans Tech Publ*, pp. 341-346.

[22] L. Meirovitch, *Methods of Analytical Dynamics*, McGraw-Hill, New York, USA, 1970.

Masoud SoltanRezaee received his Ph.D. degree in Mechanical Engineering from Tarbiat Modares University, Iran. During his Ph.D. study, he also worked in the Department of Mechanical and Automation Engineering at The Chinese University of Hong Kong. Masoud researches on the vehicle dynamics, stability analysis, biomechanics, and MEMS/NEMS. His current projects are "dynamic modeling and stability analysis of shaft systems" and "electro-thermo-mechanical behavior of smart biological micro-systems".

Mohammad-Reza Ghazavi is an Associate Professor of Mechanical Engineering at Tarbiat Modares University, Iran. He was graduated from The University of Bath in England in 1992. His main focus is on the stability analysis and nonlinear dynamics of different mechanical systems. He also researches the modeling of various mechanisms in addition to machining.

Asghar Najafi received his Ph.D. degree in Mechanical Engineering from Tarbiat Modares University, Iran. His major fields are vibration and stability analysis of rotating machines. Currently, he works at the Department of Mechanical Rotary Equipment, Niroo Research Institute, Iran, as a Research Assistant Professor.

Wei-Hsin Liao received his Ph.D. in Mechanical Engineering from The Pennsylvania State University, University Park, USA. Now, he is a Professor in the Department of Mechanical and Automation Engineering at The Chinese University of Hong Kong, where he is also the founding director of the Smart Materials and Structures Laboratory. He currently serves as an Associate Editor for some journals and is a Fellow of ASME, HKIE, and IOP.

© 2019 Int. J. Mech. Eng. Rob. Res